Possible options for efficient wide-band polychromatic measurements using chopper spectrometers at pulsed sources

Kenji Nakajima[1, 2,*], *Tatsuya* Kikuchi[1, 3, 4], *Seiko* Ohira-Kawamura[1], and *Wataru* Kambara[1]

[1]Materials & Life Science Division, J-PARC Center, JAEA, Tokai, Ibaraki, Japan
[2]Materials Sciences Research Center, JAEA, Tokai, Ibaraki, Japan
[3]Research & Development HQ., Sumitomo Rubber Industries, Ltd., Kobe, Hyogo, Japan
[4]Institute of Materials Structure Science, KEK, Tsukuba, Ibaraki, Japan

Abstract. The polychromatic incident energy measurements using chopper spectrometers at pulsed sources enables us to measure dynamics with different energy resolutions, i.e., different time-windows with a single-measurement. By increasing the possible time-window for a single-measurement, the efficiency and usefulness of such measurements is enhanced. This is achieved by allowing the crossing of trajectories of different E_is from different source pulses on the time-of-flight diagram (the interveined trajectory). We will present an actual case of the interveined trajectory on AMATERAS, a cold-neutron chopper spectrometer installed at J-PARC, together with our experience. Some of our attempts to formulate the conditions for performing polychromatic E_i measurements employing interveined trajectories are discussed. These which can be applied to existing spectrometers, and considered as design criteria for future chopper spectrometers. Further related plan of AMATERAS to improve measuring efficiency is also mentioned.

1 Introduction

Direct access to quantitative measurements of the static and dynamical correlations of atoms, molecules and spins in energy and momentum spaces is one of prominent futures of the neutron scattering technique. Based on many of techniques and technologies invented so far, inelastic and quasi-elastic neutron scattering instruments have been continuously improved their performance to achieve higher and flexible resolution, higher intensity and higher efficiency, to open the door to a rich frontier of nature science.

To capture dynamics of phenomena in materials, a large coverage of different degrees of time windows is one of the keys. A legacy way to achieve such measurements is to measure the same dynamics with different neutron spectrometers having different energy resolutions. Of late, polychromatic incident energy (E_i) measurements carried out by utilizing repetition rate multiplication technique have considerably improved the efficiency of chopper spectrometers at pulsed sources [1, 2]. The polychromatic E_i technique, which has become common in chopper spectrometers in recent decades, has enabled wide-time window dynamic measurements by a single measurement, using a single spectrometer. This capability has stimulated the emergence of new types of data handling, such as the mode distribution analysis [3], which enables us to evaluate the number of modes and their characteristic time scale from quasi-elastic measurements, without making any assumptions. Then it is natural that our interest goes to seek the technique to obtain dynamical response function in wider range of time window with higher efficiency with a single measurement.

Some efforts have been made on AMATERAS, a cold-neutron chopper spectrometer installed at a pulsed source [4], to increase accessible time-windows with a single measurement condition. As it is known, by allowing the crossing of trajectories of different E_is from different source pulses on the time-of-flight (TOF) diagram, the usable width for the magnitude of E_is can be increased. We call this the interveined trajectory. The interveined trajectory is a powerful technique for spectrometers operating in the polychromatic E_i mode, and has been employed on AMATERAS along with other attempts, including to increase the number of usable E_is from the source by modifying the chopper system.

In this paper, we will present our attempts and experiences, and a plan of using AMATERAS to increase time-windows and enhance measuring efficiency in a single measurement. Measurements utilizing the interveined trajectory form the crux. Our experiences and considerations of the interveined trajectory will be described, which includes an actual case using AMATERAS. An introductory consideration, and our attempts to formulate the conditions are included. We also mention a future plan of AMATERAS to improve the efficiency of wide-band measurements by modifying the pulse shaping chopper. We hope that these will help to existing and future planned spectrometers with wide-band polychromatic E_i measurements.

* Corresponding author: kenji.nakajima@j-parc.jp

2 Bandwidth and interveined trajectory

For instruments installed at a conventional pulse neutron source, useful band width depends on the repetition rate of the source [5]. In the case of instruments utilizing a white neutron beam from the source (e.g., diffractometers, inverted geometry spectrometers and neutron imaging facilities), the band width in the wave length, $\Delta\lambda_{max}$, can be written as shown in Eq. (1).

$$\Delta\lambda_{max} = h\tau/m_n L_{tot} \quad (1)$$

where h is the Plunk constant, τ is the interval time between the source pulses, m_n is the mass of neutron, and

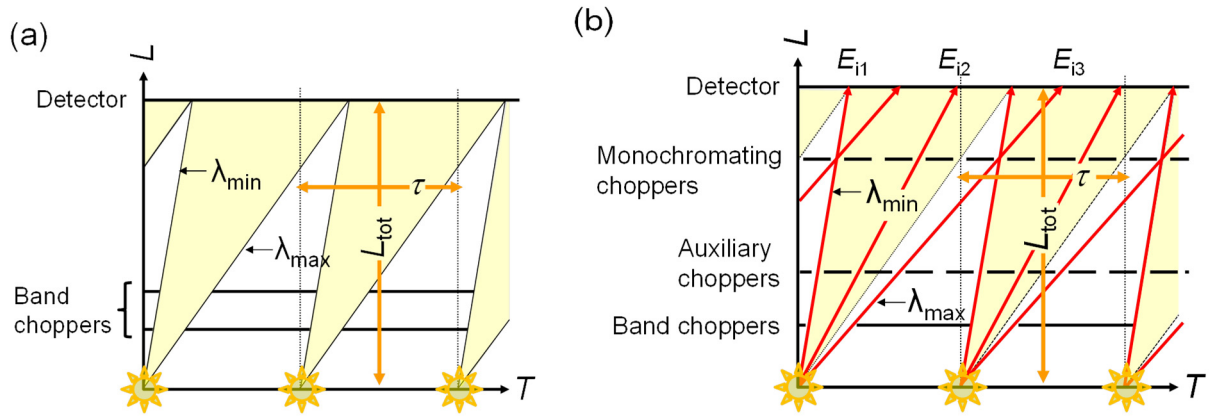

Fig. 1. A TOF diagram explaining the possible band width at a pulsed source. (a) In the conventional case. Available maximum time window at the detector position is t, the interval time of the source pulses. The possible wave length band, $\Delta\lambda = \lambda_{max} - \lambda_{min}$ is determined by t and the total flight distance, L_{tot}. (b) The interveined trajectory case. Three E_is are selected in the figure, namely E_{i1}, E_{i2}, and E_{i3}. Here, trajectories of E_{i1} and E_{i3} are crossing at the same monochromating chopper opening, i.e., the interveined trajectory. The effective wave length band, $\Delta\lambda = \lambda_{max} - \lambda_{min}$ is wider than it is in the conventional case. The auxiliary chopper in the figure is optional. In the figures, L and T stand for the flight path length and the time-of-flight, respectively.

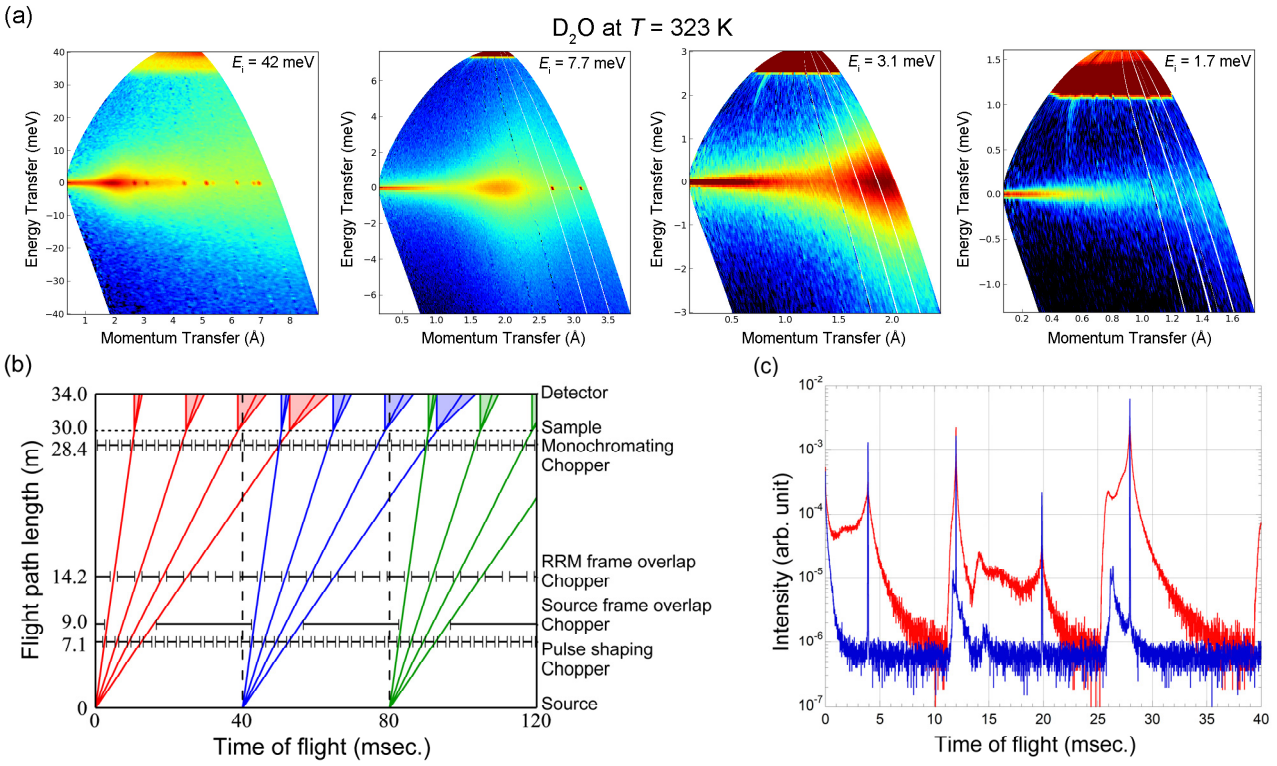

Fig. 2. An actual use of the interveined trajectory in AMATERAS at J-PARC, where we could realize the measurements with four E_is—42, 7.7, 3.1, and 1.7 meV—and energy resolutions in the 0.9–0.01 meV range, which corresponds to 0.02 ps–500 ps time windows. (a) Example of data obtained from D_2O measurements at 323 K. (b) Time-of-flight (TOF) diagram of this condition (E_is from the $T < 0$ are omitted in the figure). (c) TOF spectrum measured of D_2O data shown in (a) (red line) together with a vanadium cylinder at room temperature data (blue line). The data obtained at the equatorial position detector pixels were used. Note that AMATERAS has another band chopper at 13.7 m position, which is not used in this condition, and is therefore removed in panel (b). It should be noted that the value of the flight path length from the source to the detector shown in panel (b) is at the equatorial position of the detector bank [4]. Actual distance from the sample to the detector pixels spreads from 4 m to 4.4 m.

Table 1. AMATERAS chopper configuration

Role [7]	Position from the source	Maximum revolution	Number of disks	Slit size or opening angle
Pulse-shaping chopper	7.1 m	350 Hz	2 (counter-rotating)	Slit size: 30 mm
Monochromating chopper	28.4 m	350 Hz	2 (counter-rotating)	Slit size: 10 mm and 30 mm
RRM frame overlap chopper	14.2 m	350 Hz	1	Slit size: 30 mm
Source frame overlap chopper 1	9 m	25 Hz	2 (co-rotating)	Open angle: 0°−175° (variable)
Source frame overlap chopper 2	13.7 m	25 Hz	2 (co-rotating)	Open angle: 0°−175° (variable)

L_{tot} is the total flight path length. The arrangement is shown in Fig. 1 (a). If one needs the band width to be longer than that in Eq. (1), one can discard several source pulses by some means. Removing one of two pulses can double it, and removing two of three can triple it. This is usually done with instruments upon request. However, it sacrifices time averaged neutron flux.

It is known to those who are experienced with polychromatic E_i measurements that we can employ an alternative way to extend $\Delta\lambda$, in the case of chopper spectrometers. By allowing trajectories of different E_is from different source pulses to cross each other on the TOF diagram, we can have extension of the effective band width, that is interveined trajectory. An example is shown in Fig. 1 (b), in which allowing different E_is to transmit the same opening of the monochromating chopper, that is one of the ways to realize an interveined trajectory. Using an interveined trajectory, a chopper spectrometer can select the set of E_is in the range of the band width wider than in the conventional case.

An interveined trajectory is employed at AMATERAS in actual measurements. We have already reported the result of measurement on D_2O at 273 K in our earlier manuscript [4]. Here, we show another example, i.e., the result of measurement on D_2O at 323 K in Fig. 2 (a). Data taken with four different E_is, namely 42, 7.7, 3.1, and 1.7 meV, were obtained by a single measurement. Measurement with energy resolutions from 0.9 meV to 0.01 meV corresponds to 0.02 ps–500 ps time windows, were realized. Variation of four E_is in wave length (effective band width) is 5.6 Å. The value is wider than the maximum band width defined by Eq. (1), 4.7 Å for t = 40 ms and L_{tot} = 34 m. The time-of-flight (TOF) diagram for this condition is shown in Fig. 2(b). Detailed information on the AMATERAS disk-choppers can be found in the reports [4, 6], while simple information is shown in Table 1. The details on the roles of each chopper written can be found in Ref. 7. The pulse-shaping chopper, the monochromating chopper, the RRM frame overlap chopper, and the source frame overlap chopper 1 were operated at revolution rates 300 Hz, 300Hz, 150 Hz, and 25 Hz, respectively. We did not operate (i.e., stopped at the open position) the source frame overlap chopper 2 in this condition. We present D_2O spectrum data with vanadium data in Fig. 2 (c). Overlapping of signals (contamination) on the TOF spectrum is important for measurements on chopper spectrometers [8]. We will discuss the contamination issue later.

We obtained some experiences on the interveined trajectory measurements on AMATERAS. An auxiliary chopper shown in Fig. 1 (b) is optional. Although one can implement an interveined trajectory without this chopper (when the monochromating chopper runs at half of the frequency, we can remove the auxiliary chopper of Fig. 1 (b)), by using such choppers to remove selected pulses from the source, we can increase possible options of operation modes of the monochromating chopper. For this purpose, we sometime use the RRM frame overlap chopper. A fan chopper [9], a selective pulse suppression chopper [10] or a more flexible type of selective pulse suppression chopper [11] may provide more flexibility. On the other hand, slow disk-choppers with variable opening are indispensable. Since the width of the band definition in experiments with/without interveined trajectories are different, the ability to define different bandwidths is needed in slow disk-choppers. Ultimately, the redundancy of chopper systems is important. The flexibility allows us to perform new types of experiments, even those not considered before construction.

3 Some of attempts to formulate the interveined trajectory

This section documents our experience with the algebra used to find conditions suitable for the interveined trajectory in actual spectrometers. Our attempts to formulate the relationship between the pulse repetition rate of the source, the flight distances of the spectrometer, the chopper frequency, and other relevant parameters in two selected conditions for carrying out interveined trajectory measurements, are presented. These are just examples. One can extend these ideas upon one's requests for constructing new spectrometers or make a design of new types of measurements.

In this section, we assume the following *a priori* conditions.

i. The monochromating chopper is synchronized with the source pulse, and it opens at least once in the time period τ.
ii. Choppers with irregular opening timing (e.g., a fan chopper and a selective pulse suppression chopper), are not used.

3.1 Case I: Near-elastic (equal time interval case)

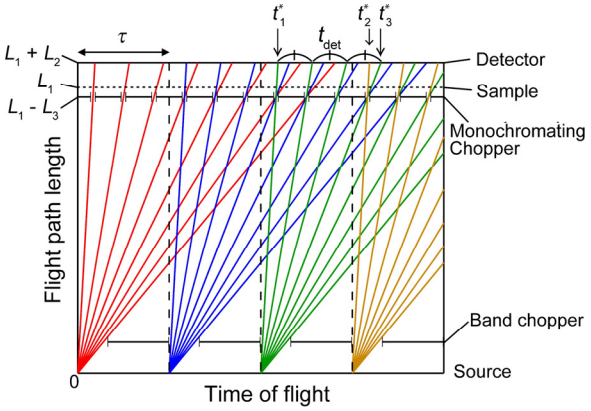

Fig. 3. Example of the case to obtain E_is arriving at the detector position at a regular interval. In this figure, the combination of parameters $n_f = 3$, $n_i = 3$, $n_p = 8$, and $n_d = 1$ is considered. Detail can be seen in the text. E_is from the time < 0 are omitted in the figure.

As one of the simplest examples, let us consider the case obtaining all E_is arriving at the detector position at regular intervals. If focusing on elastic and/or near elastic channels (e.g., elastic incoherent structure factor (EISF) measurements), we can consider this simple case, in which it is not necessary to consider the time window for the inelastic region. As case I is simple, it may not have many applications but is a good for an introduction.

An example of such a case is in Fig. 3. Here after, it is defined as follows.

L_1: Distance from the source to the sample,
L_2: Distance from the sample to the detector,
L_3: Distance from the monochromating chopper to the sample.

In addition, we introduce the following parameters.

n_p: Number of E_is from one source pulse,
n_f: Number of frames that E_is from one source pulse spread over,
n_i: Maximum number of E_is from one source can be accommodated in one frame,
t_{det}: Time interval between E_is from one source pulse at the detector position.

The relationship between these parameters is illustrated using the following ceiling functions.

$$n_f = \mathrm{ceil}\left(\frac{n_p t_{\mathrm{det}}}{\tau}\right), \quad (2)$$

$$n_i = \mathrm{ceil}\left(\frac{\tau}{t_{det}}\right). \quad (3)$$

A priori conditions guarantee that $n_p \geq n_f$.

An example in Fig. 3 corresponds to $n_p = 8$, $n_f = 3$, and $n_i = 3$. We also introduce some definitions regarding the order of arrival of neutrons from different source pulses.

N_n: n is an integer index for the E_i to identify the source pulse from which it emerged. The E_i of N_1 means the E_i emerged from the most recent source pulse. The E_i of N_2 means the E_i emerged from the penultimate source pulse, and so on.

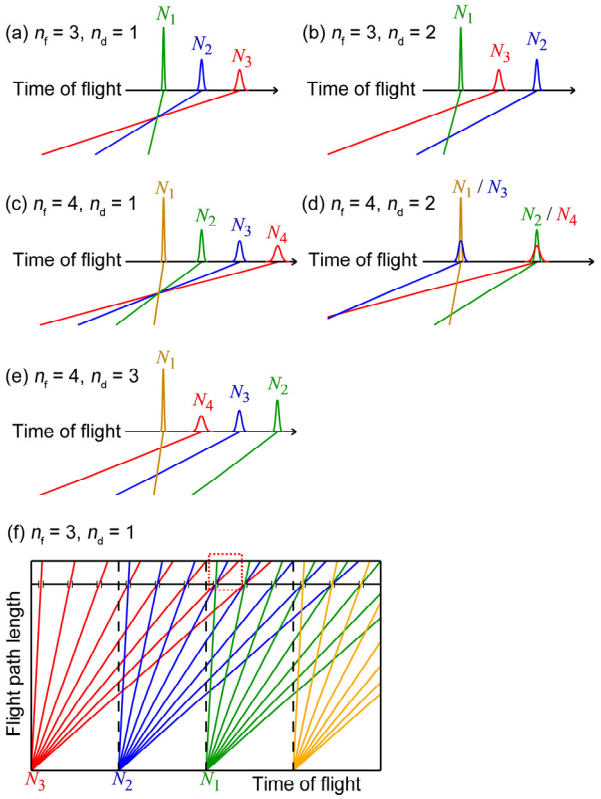

Fig. 4. Some of sequences of E_i as examples to explain definition of Nn and n_d. Possible sequences of E_is are described in the cases of n_f = 3 ((a) and (b)) and 4 ((c) ~ (e)). Corresponding n_ds are shown together. When n_d and n_f are not relatively prime numbers, neutrons from different source pulses arrive at same time at the detector position as can be seen in (d). (f) The full TOF diagram of the case (a) ($n_f = 3$, $n_d = 1$). E_is from the time < 0 are omitted in the figure. The panel (a) corresponds to the area surrounded by the red square in (f).

n_d: The index stands for the order of the arrival at the detector position of E_i of N_2 counted from the earliest E_i of N_1.

Examples are shown in Fig. 4. When $n_i \geq 3$, there are choices for a permutation-combination arrangement in the order of arriving E_is from different source pulses. Some of examples are shown in Fig. 4 for the cases of $n_f = 3$ and 4. Once n_f and n_d are determined, orders of N_n ($n \geq 3$) are automatically determined when *a priori* conditions are satisfied. When n_d and n_f are not relatively prime numbers, neutrons from different source pulses arrive simultaneously at the detector, as can be seen in Fig. 4 (d).

For E_is arriving at the detector at regular intervals, we have to accommodate E_is of N_2 ~ N_{nf} in the time window between two consecutive E_is of N_1s at the maximum. That means the time interval of all E_is is t_{det}/n_f. Therefore, the relationship is defined as follows.

$$\tau = \left(n_i - \frac{n_d}{n_f}\right) t_{\mathrm{det}} \quad (4)$$

An empirical approach can help explain Eq. (4). One can see the timing of the highest E_is from two consecutive source pulses, t^*_1 and t^*_2 in Fig. 3. Then, $t^*_2 - t^*_1$ is τ within *a priori* conditions. Conversely, after t^*_2, (n_i+1)th E_i from the earlier source pulse arrives at t^*_3 and t^*_3 is equal to (n_i+1)×t_{det}. To go back from t^*_3 to t^*_2, the duration

(interval time of E_is at the detector position)×n_d should be subtracted from t^*_3. Since the time interval of all E_is is t_{det}/n_f, τ is $((n_i+1)\times t_{det})-(n_d\times(t_{det}/n_f))$, that is Eq. (4).

There is choice in the location of the monochromating chopper. For example, in Fig. 1 (b), when we remove the monochromating chopper, only with the auxiliary chopper in the figure, we can obtain the same set of E_is, if we can ignore the resolution which becomes worse substantially with shorter distance from the source to the monochromating chopper. Under assumption of *a priori* conditions, one of the effective locations for the monochromating chopper in case I may be the position at which the interval between two consecutive opening timing of the monochromating chopper can be the longest. The longer interval time chopper location means more downstream position. Slower revolution rate of the chopper makes the resolution coarse. However, one may be able to obtain higher resolution by multiplying the revolution rate. That is the position on the TOF diagram at which number of the crossing of lines of E_is is maximum. This situation is described in Fig. 3. We define this location by L^*_3.

L^*_3: Distance from the monochromating chopper to the sample, where the interval between two consecutive opening timing of the chopper can be the longest.

Using L^*_3, we can show equations that are relevant to designing spectrometer dimensions and the lowest revolution rate of the chopper as follows.

$$\frac{L_2+L_3^*}{L_1-L_3^*} = \frac{t_{\mathrm{det}}/n_{\mathrm{f}}}{\tau} n_{\mathrm{d}} = \frac{n_{\mathrm{d}}}{n_{\mathrm{f}} n_{\mathrm{i}} - n_{\mathrm{d}}}, \quad (5)$$

$$f^*_{\mathrm{chop}} = n_i \nu. \quad (6)$$

Here, $f_{chop}{}^*$ is the frequency of the monochromating chopper located at $L_3{}^*$ and ν is the frequency of the source pulse. Eqs. (5) and (6) offer a choice of conditions for obtaining E_is at the same interval time at the detector position by utilizing the interveined trajectory with a simple chopper set—i.e., one monochromating chopper and band chopper, and no pulse removing choppers.

3.2 Case II: Inelastic case

Case I is an apt exercise for considering the interveined trajectory. However, it does not fit to inelastic measurements, which is the main task of chopper spectrometers. In inelastic measurements, the arrival time of neutrons scattered by inelastic processes is spread asymmetrically before and after the elastic channel. Moreover, time windows depend on the magnitude of E_i itself. Therefore, the regular interval time of case I is not suitable. In case II, we consider asymmetric arrival times and E_i dependent time spreading.

First, we define contamination of the inelastic spectra from other E_is. For simplify, we assume that (a) the contamination on inelastic spectrum from the specific E_i (E_{i0}) is caused only by the E_i (E_{i+}) arriving next to E_{i0}, and we ignore the contamination from the E_i (E_{i-}) arriving before the E_{i0}. We also assume that (b) the contamination starts from the time that E_{i+} arrives at the sample position. Cases that deviate from the above assumption are expected too. Regarding to assumption (a), contaminations from E_{i-} is less effective, since the inelastic signals are spreading in rather longer time ranges in the case of the neutron-energy-loss side. However, it depends on the intensity of the inelastic signals; if they have high intensity, we cannot ignore them [8]. About assumption (b), the time when the contamination from E_{i+} starts depends on the sample (scatterer) and temperature of it (the Bose factor). The actual contamination starts slightly later in some cases as we mention in Sec. 3.3. Although there are exceptions in our assumptions, our experience (and that of others working on inelastic spectrometers) suggests that these assumptions are reasonable. In addition, such simplification allows us to define the conditions using simple algebra, as we will show here.

We consider the inelastic spectra in only the neutron-energy-loss side. We define the largest energy transfer, ΔE, which is clean from the contamination as follow.

$$\Delta E \leq r E_i. \quad (7)$$

Our task then is to find the condition to optimize the set of r for possible E_is to determine the most usable spectrometer parameters. By utilizing the idea used in case I, we can derive the following equation.

$$\tau = \left(n_i - \frac{n_d}{n_f}\right) t_{\mathrm{sam}} + \Delta t \quad (8)$$

where t_{sam} is the time interval of E_is emitted from the same source pulse at the sample position, which is an analog of t_{det}. One should note that, under *a priori* conditions, what we can do is only adjusting Δt by changing the spectrometer parameters. When $\Delta t = 0$, all E_is, including those from different source pulses, arrive at the sample position at regular intervals. By changing Δt, the magnitude of r can be varied. After Δt was introduced, even in the case of n_d and n_f, which are not relative prime numbers, neutrons from different source pulses do not arrive at exactly same time at the detector position if Δt is not 0. However, these neutrons arrive closely and cannot again be used.

There can be various criteria to optimize the set of r. The lower E_i needs a wider time spread. Therefore, it is natural to focus on the r (r_L) for the lowest E_i (E_{iL}). Comparing r_L with r values of other higher E_is, leads to ideas for optimizing the set of r values. We compare r_L with r of the E_i (E_{iL-}) arrived at the sample position just before E_{iL}. We will find the condition to make rs for E_{iL} and E_{iL-} equal, and that is our criterion. We understand that this criterion may not be the best. We may have to compare with r values of all E_is. Other more sophisticated conditions, e.g., giving weights to some of specific E_is, which need wider windows to cover the signals that need to be measured may have to be employed. However, our simple criterion should work in most of experiments as a standard to determine the condition for the interveined trajectory measurements. Moreover, this criterion allows

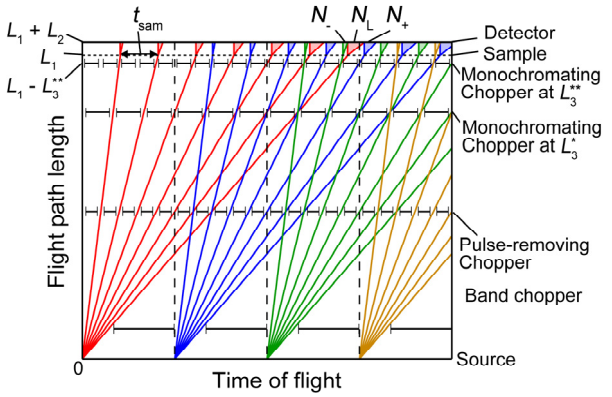

Fig. 5. Example of optimized polychromatic E_i measurements considering time spreading of neutrons' arrival time by inelastic scattering. Corresponding parameters are $n_f = 3$, $n_i = 3$, $n_d = 2$, and $s = 7$ (or $s' = 2.872$). Two possible monochromating chopper positions are shown at L_3^* and L_3^{**}. When the monochromating chopper at L_3^{**} is employed, a pulse-removing chopper should be introduced (see text). E_is from the time < 0 are omitted in the figure.

us to express the condition using relatively simple algebra. The condition depends on n_d and n_f. Here, we concentrate on the case of $n_d = n_f - 1$. That is the case used in the actual measurements on AMATERAS (Fig. 2) and, in this condition, it is easy to obtain the necessary formulas, as we will see later.

An example is shown in Fig. 5, in which n_f, n_i, and n_d are 3, 3, and 2, respectively. In this case, we introduce a pulse-removing chopper in addition to band choppers. One should note that, r values for other E_is are larger than that for E_{iL} and E_{iL-} ($= r_L$) accidentally.

We will express our criterion using equations. The flight time of E_{iL} from the source to the sample position, t_L is written as follows.

$$t_L = L_1\sqrt{\frac{m_n}{2}\cdot\frac{1}{E_{iL}}} \tag{9}$$

The possible minimum scattered (final) energy from E_{iL} is $(1\text{-}r_L)E_{iL}$ from the definition (Eq. (7)). The time from the source to the detector position, at which the maximum energy transfer in neutron-energy-loss side is detected, (t_{L_tot}) is given in Eq. (10).

$$t_{L_{tot}} = L_1\sqrt{\frac{m_n}{2}\cdot\frac{1}{E_{iL}}} + L_2\sqrt{\frac{m_n}{2}\cdot\frac{1}{(1-r_L)E_{iL}}},$$
$$= (1+\chi)t_L, \tag{10}$$
$$\chi = \frac{L_2}{L_1}\frac{1}{\sqrt{1-r_L}}. \tag{11}$$

The condition $n_d = n_f - 1$ gives the following constraints. The E_i (E_{iL+}) arriving at the sample position next to E_{iL} is from the source pulse next to where E_{iL} is emitted from. The flight time of E_{iL+} from the source to the sample is $t_L\text{-}(n_i - 1)t_{sam}$. When we count the time from the source pulse which E_{iL} emerged from, we should add τ. According to our criterion, this time coincides with t_{L_tot}.

$$(1+\chi)t_L = t_L - (n_i - 1)t_{sam} + \tau. \tag{12}$$

Then we consider E_{iL-} which is emitted from the source pulse $(n_f - 1) = n_d$ times next to that E_{iL} started from, under the condition of $n_d = n_f - 1$. The flight time of E_{iL-} from the source to the sample is $t_L - ((n_f - 1)(n_i - 1) + 1)t_{sam}$. When we count the time from the source pulse which E_{iL} emerged from, we should add $(n_f - 1)\tau$. That gives the following equation.

$$(1+\chi)\left[t_L - \{(n_f-1)(n_i-1)+1\}t_{sam}\right] + (n_f-1)\tau = t_L \tag{13}$$

If Eqs. (12) and (13) are true, χ can be written as following.

$$\chi = \frac{1}{n_f s-(n_f-1)(n_i-1)-1}, \tag{14}$$
$$s = t_L/t_{sam}. \tag{15}$$

In Fig. 5, the value s is 7. From our experience, one may want to handle the value s, as an independent parameter. Then, the expression of t_{sam} as a function of other relevant parameters including s might be useful. From Eq. (12), we can write down t_{sam} as Eq. (16),

$$t_{sam} = \frac{1}{\chi s+n_i-1}\tau\,. \tag{16}$$

By combining Eqs. (14) and (16), we get expression.

$$t_{sam} = \frac{n_f s-(n_f-1)(n_i-1)-1}{(n_f n_i-n_f+1)s-\{(n_f-1)(n_i-1)+1\}(n_i-1)}\tau. \tag{17}$$

To decide the spectrometer parameters, the standards of distance, time and target slope of trajectory are required. For example, when τ, L_1, r_L, and s are given, one can choose the combination of n_f and n_i. The parameter χ will be determined from Eqs. (16) and (17). In addition, L_2 will be given by Eq. (11). Other combinations are also possible.

About the location of the monochromating chopper, L_3 and the chopper frequency, f_{chop}, evaluating values of L_3^* and f_{chop}^* defined in Sec. 3.1 under the case II condition is one of several candidates (the position indicated as L_3^* in Fig. 5). However, the position L_3^* at which the maximum number of trajectories of E_is crossed might be not appropriate in some cases. In the case of Fig. 5, there is a more plausible downstream position for L_3 (L_3^{**}), as shown in the figure, which may be better for the resolution of the chopper spectrometer. We define L_3^{**} as the location at which trajectories of E_{iL-} and E_{iL} cross over together at the most downstream position. Such L_3^{**} and corresponding the lowest chopper frequency f_{chop}^{**} can be derived easily in the current case, and can be obtained by following equations.

$$\frac{L_1-L_3^{**}}{L_1} = \frac{\{(n_f-1)(n_i-1)+1\}t_{sam}}{(n_f-1)\tau},$$
$$= \frac{(n_f-1)(\chi s+n_i-1)}{(n_f-1)(n_i-1)+1}, \tag{18}$$

or,

$$\frac{L_3^{**}}{L_1} = \frac{1-\chi(n_f-1)s}{(n_f-1)(n_i-1)+1},$$
$$= \frac{s-(n_f-1)(n_i-1)-1}{\{n_f s-(n_f-1)(n_i-1)-1\}\{(n_f-1)(n_i-1)+1\}}, \tag{19}$$

$$f_{chop}^{**} = \{(n_f - 1)(n_i - 1) + 1\}\nu. \quad (20)$$

Here we used Eqs. (16) and (14) to obtain the final lines of Eqs. (18) and (19). As mentioned previously, we need auxiliary choppers for this condition, as shown in Fig. 5.

In the actual design process, it might be difficult to decide s before determining t_{sam}. In such a case, another parameter, s', can be an alternative key parameter.

$$s' = t_L/\tau. \quad (21)$$

One can convert from s to s' by using following formula.

$$s' = \frac{n_f s^2 - \{(n_f-1)(n_i-1)+1\}s}{(n_f n_i - n_f + 1)s - \{(n_f-1)(n_i-1)+1\}(n_i-1)} \quad (22)$$

3.3 Reality of case II

The reality of case II can be seen in actual measurements using AMATERAS.

The condition shown in Fig. 2 is almost the ideal case of the combination of the parameters $n_f = 2$, $n_i = 3$, $n_d = 1$, $s = 3.75$, and $s' = 1.32$. The calculated value of r from Eqs. (11) and (14) (r_{calc}) is 0.64. The values calculated from the actual TOF (r_{TOF}) are 0.603 and 0.648 for $E_i = 42$ and 1.7 meV, respectively. The deviation of r_{TOF} from r_{calc} indicates the deviation of the real case from the ideal case. This deviation can also be found in the location of the monochromating chopper. The value L_3 is 1.6 m in AMATERAS, while Eq. (19) gives 1.67 m.

In the actual analysis on D_2O at 323 K data, we found that we can analyze data roughly up to $r_{real} = 0.74$ and 0.61 for $E_i = 42$ meV and 1.7 meV, respectively (see also Fig. 2 (a)). As we mentioned, in the actual case, the contamination on the inelastic spectrum from E_{i0} by the next E_i (E_{i+}) does not exactly starts from the time when E_{i+} arrive at the sample position. It depends on the sample (scatterer) and temperature of it. If it has enough cross-section in higher energy transfer, and if the temperature is high enough to result in a higher Bose factor, the starting time of the contamination becomes close to the time when E_{i+} arrive at the sample position. The sample of D_2O and a temperature of 323 K are not enough to deliver enough intensity in the neutron-energy-gain side, and that is the case of $E_i = 42$ meV for which $r_{real} > r_{TOF}$, r_{calc}. The r_{real} value for $E_i = 1.7$ meV needs another explanation. In the calculation, we adapted the value $L_2 = 4$ m, which is the distance from the sample position to the equatorial position of detector bank. AMATERAS employs 3 m length (2.9 m in the active length) 1-dimentional position sensitive detectors and the distance from the sample to the detector pixel is spreading from 4 m to 4.4 m at the maximum. Difference in calculated and real distance gives deviations from the resulting values, especially in the case of the slow neutron (i.e., lower energy neutron) E_is. If one wants to avoid such a situation, the average value, or the maximum value for a naive treatment, of L_2 may be used.

4 Summary and a further plan of AMATERAS

Our attempts, experiences, and learnings from performing interveined trajectory measurements on AMATERAS are described here. That is one of our efforts to enhance the efficiency of wide-band polychromatic E_i measurements. By allowing trajectories of the different E_is from the different source pulses to cross together on the TOF diagram, we can extend useful bandwidth (width of variation of E_is) of chopper spectrometers installed at pulsed neutron sources. We learnt that the interveined trajectory used together with the polychromatic E_i

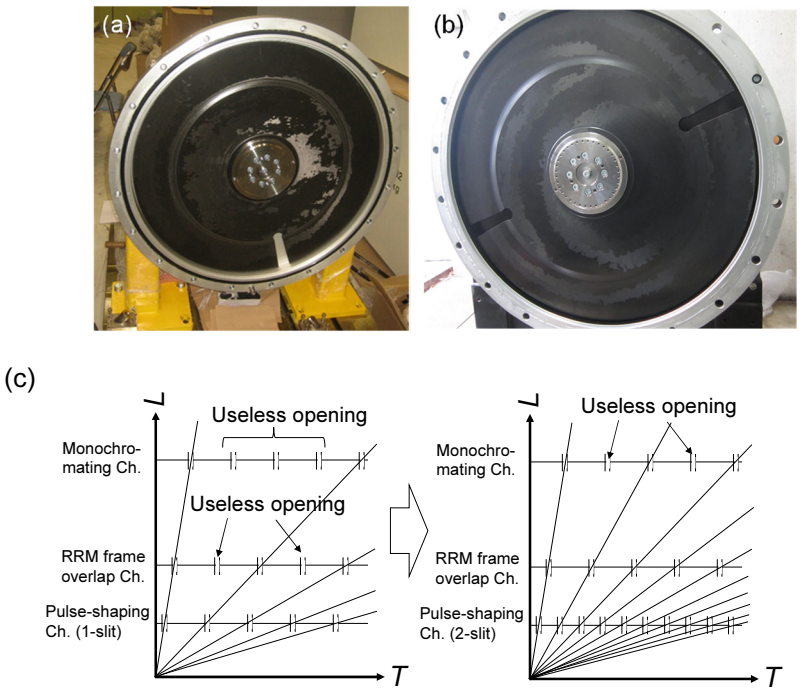

Fig. 6. Disks for the pulse shaping chopper of AMATERAS. (a) A single slit disk, which is currently used. (b) A double slit disk newly prepared (on a test-bench). (c) Schematic image of improvement by doubling the slit of the pulse shaping chopper at AMATERAS. In (c), L and T stand for the flight path length and the time-of-flight, respectively.

measurement can be a powerful tool for efficient measurements on spectrometers. In AMATERAS's case, we can realize measurements with energy resolutions from 0.9 meV to 0.01 meV, which corresponds to 0.02–500 ps time windows. We adequately demonstrated our consideration of the required conditions to realize the interveined trajectory. Based on our experience, we introduced two types of attempts to formulate spectrometer conditions. We understand that these are simplistic ideas, and we hope that a more sophisticated and generalized methodology will be developed in future.

Before constructing AMATERAS, we did not consider the possibility of interveined trajectory measurements on this spectrometer. We could still carry out the intervein trajectory measurements with the help of the equations we showed, which means that the conditions considered here have some robustness in real life. Moreover, as we mentioned, to employ the interveined trajectory more flexibly, several optional devices are required. One is an auxiliary chopper to remove pulses. The other one is flexible opening band choppers. Redundancy and flexibility in the chopper system of the spectrometer enabled us to carry out new types measurements, which we had not planned on before construction.

Here we also mention about data reduction processes done for the interveined trajectory measurements on AMATERAS. We are using data reduction software '*Utsusemi*' [12], which is commonly used at MLF. '*Utsusemi*' has no special cares for the interveined trajectories. Once the values of all E_is are correctly identified, that is done by manually in our case, the processes for the interveined trajectories are the same as those for conventional polychromatic E_i measurements. When the data reduction process includes automatic E_i determination process, one may need a care for the interveined trajectories.

Needless to say, not only extending the possible time window, but also increasing the usable number of E_is is important in efficient polychromatic E_i measurements. In the case of AMATERAS, the opening of the pulse shaping chopper is one of the bottlenecks in obtaining the number of E_is. To solve this problem, we are preparing a double slit disk for the pulse shaping chopper (Fig. 6), which is under performance testing. Since the ratio of the distance from the source to the monochromating chopper to that to the pulse shaping chopper is 28.4 m/7.1 m = 4, a disk with four slits is ideal to eliminate possible 'useless' openings completely. Therefore, a 4-slit disk will be in the scope after further development.

We hope that the experiences we have recorded here will assist in carrying out wide-band polychromatic E_i measurements on existing and planned spectrometers around the world.

We would like to thank the rest of the AMATERAS team members, Maiko Kofu and Naoki Murai for the discussions and their help in carrying out related works. We thank to Ryoichi Kajimoto for the helpful discussions and valuable suggestions. We also acknowledge the staff members of MLF, J-PARC, for their help in development and implementation of disk-choppers. The work was supported by JSPS KAKENHI Grant Number 24510133 and 18K11927. Data shown in this paper were obtained by experiments performed at MLF, J-PARC as a part of instrumental proposal 2009A0092.

References

1. M. Russina, F. Mezei, Nucl. Instrum. Methods Phys. Res.: Sect. A **604**, 624 (2009) and references therein
2. M. Nakamura, R. Kajimoto, Y. Inamura, F. Mizuno, M. Fujita, T. Yokoo, M. Arai, J. Phys. Soc. Jpn. **78**, 093002 (2009)
3. T. Kikuchi, K. Nakajima, S. Ohira-Kawamura, Y. Inamura, O. Yamamuro, M. Kofu, Y. Kawakita, K. Suzuya, M. Nakamura, M. Arai, Phys. Rev. E **87**, 062314 (2013)
4. K. Nakajima, S. Ohira-Kawamura, T. Kikuchi, M. Nakamura, R. Kajimoto, Y. Inamura, N. Takahashi, K. Aizawa, K. Suzuya, K. Shibata, T. Nakatani, K. Soyama, R. Maruyama, H. Tanaka, W. Kambara, T. Iwahashi, Y. Itoh, T. Osakabe, S. Wakimoto, K. Kakurai, F. Maekawa, M. Harada, K. Oikawa, R. E. Lechner, F. Mezei, M. Arai, J. Phys. Soc. Jpn. **80** suppl. B, SB028 (2011)
5. C. G. Windor, *Pulsed Neutron Scattering*, London: Taylar & Francis Ltd. (1981)
6. K. Nakajima, Y. Kawakita, S. Itoh, J. Abe, K. Aizawa, H. Aoki, H. Endo, M. Fujita, K. Funakoshi, W. Gong, M. Harada, S. Harjo, T. Hattori, M. Hino, T. Honda, A. Hoshikawa, K. Ikeda, T. Ino, T. Ishigaki, Y. Ishikawa, H. Iwase, T. Kai, R. Kajimoto, T. Kamiyama, N. Kaneko, D. Kawana, S. Ohira-Kawamura, T. Kawasaki, A. Kimura, R. Kiyanagi, K. Kojima, K. Kusaka, S. Lee, S. Machida, T. Masuda, K. Mishima, K. Mitamura, M. Nakamura, S. Nakamura, A. Nakao, T. Oda, T. Ohhara, K. Ohishi, H. Ohshita, K. Oikawa, T. Otomo, A. Sano-Furukawa, K. Shibata, T. Shinohara, K. Soyama, J. Suzuki, K. Suzuya, A. Takahara, S. Takata, M. Takeda, Y. Toh, S. Torii, N. Torikai, N. L. Yamada, T. Yamada, D. Yamazaki, T. Yokoo, M. Yonemura and H. Yoshizawa, Quantum Beam Science **1**, 9-64 (2017)
7. F. Mezei, J. Phys. Soc. Jpn., **82**, SA025 (2013)
8. R. Kajimoto, M. Nakamura, K. Nakajima, M. Fujita, Nucl. Instrum. Methods Phys. Res., Sect. A, **729**, 365 (2013)
9. N. Violini, J. Voigt, S. Pasini, T. Brueckel, Nucl. Instr. Meth. A, **736** 31 (2014)
10. M. Russina, F. Mezei, G. Kali, J. Phys.: Conf. Ser., **340**, 012018 (2012)
11. G. Sala, M. Mourigal, C. Boone, N. P. Butch, A. D. Christianson, O. Delaire, A. J. DeSantis, C. L. Hart, R. P. Hermann, T. Huegle, D. N. Kent,J. Y. Y. Lin, M. D. Lumsden, M. E. Manley, D. G. Quirinale, M. B. Stone, Y. Z, Rev. Sci. Instrum. **93**, 065109 (2022)
12. Yasuhiro Inamura, Takeshi Nakatani, Jiro Suzuki, Toshiya Otomo, J. Phys. Soc. Jpn. **82**, SA031 (2013)